

Crystal structure of D-stereospecific amidohydrolase from *Streptomyces* sp. 82F2 – insight into the structural factors for substrate specificity

Jiro Arima¹, Kana Shimone¹, Kazusa Miyatani¹, Yuka Tsunehara¹, Yoshitaka Isoda², Tomoya Hino³ and Shingo Nagano³

¹ Department of Agricultural, Biological, and Environmental Sciences, Faculty of Agriculture, Tottori University, Japan

² United Graduate School of Agricultural Sciences, Tottori University, Japan

³ Department of Chemistry and Biotechnology, Graduate School of Engineering, Tottori University, Japan

Keywords

acyl acceptor; amide bond formation; aminolysis; crystal structure; D-stereospecific amidohydrolase

Correspondence

J. Arima, Department of Agricultural, Biological, and Environmental Sciences, Faculty of Agriculture, Tottori University, Tottori 680-8553, Japan

Fax: +81 857 31 5347

Tel: +81 857 31 5363

E-mail: arima@muses.tottori-u.ac.jp

and

S. Nagano, Department of Chemistry and Biotechnology, Graduate School of Engineering, Tottori University, Tottori 680-8552, Japan

Fax/Tel: +81 857 31 5273

E-mail: snagano@bio.tottori-u.ac.jp

(Received 13 August 2015, revised 17 October 2015, accepted 26 October 2015)

doi:10.1111/febs.13579

D-Stereospecific amidohydrolase (DAH) from *Streptomyces* sp. 82F2, which catalyzes amide bond formation from D-aminoacyl esters and L-amino acids (aminolysis), can be used to synthesize short peptides with a DL-configuration. We found that DAH can use 1,8-diaminooctane and other amino compounds as acyl acceptors in the aminolysis reaction. Low concentrations of 1,8-diaminooctane inhibited acyl-DAH intermediate formation. By contrast, excess 1,8-diaminooctane promoted aminolysis by DAH, producing D-Phe-1,8-diaminooctane via nucleophilic attack of the diamine on enzyme-bound D-Phe. To clarify the mechanism of substrate specificity and amide bond formation by DAH, the crystal structure of the enzyme that binds 1,8-diaminooctane was determined at a resolution of 1.49 Å. Comparison of the DAH crystal structure with those of other members of the S12 peptidase family indicated that the substrate specificity of DAH arises from its active site structure. The 1,8-diaminooctane molecule binds at the entrance of the active site pocket. The electrostatic density map showed that another potential 1,8-diaminooctane binding site, probably with lower affinity, is present close to the active site. The enzyme kinetics and structural comparisons suggest that the location of enzyme-bound diamine can explain the inhibition of the acyl-enzyme intermediate formation, although the bound diamine is too far from the active site for aminolysis. Despite difficulty in locating the diamine binding site for aminolysis definitively, we propose that the excess diamine also binds at or near the second binding site to attack the acyl-enzyme intermediate during aminolysis.

Database

The coordinates and structure factors for D-stereospecific amidohydrolase have been deposited in the Protein Data Bank at the Research Collaboratory for Structural Bioinformatics under code: [3WWX](http://www.rcsb.org/pdb/entry/3WWX).

Introduction

Peptidases play vital physiological roles through the biosynthesis, degradation and regulation of peptides or proteins. Rawlings *et al.* [1] classified 400 000 pepti-

dases into 55 clans and 244 families based on their primary structures in the MEROPS database (<http://merops.sanger.ac.uk>). Peptidases are also classified by

Abbreviations

DAA, D-amino acid amidase; DAH, D-stereospecific amidohydrolase; OBzl, benzyl ester; pNA, *p*-nitroanilide; UPLC, ultra-performance liquid chromatography.

the nucleophile in the active site (e.g. as serine, threonine, cysteine, aspartate, glutamate or metal peptidases). Serine peptidases, which are classified into 53 families (S1–S81 in MEROPS), account for over 30% of the sequences in MEROPS. Although many peptidases cleave L-amino acid peptide bonds, some peptidases prefer peptides consisting of D-amino acids as a substrate. The database also contains enzymes that can cleave aminoacyl amide and ester bonds.

The most studied active site in serine peptidase is the classic Ser/His/Asp catalytic triad [2]. Variations in the active site architectures, including the Ser/Ser/Lys triad and the Ser/Lys dyad, have also been reported [3–5]. In the catalytic mechanism of all known serine peptidases, a covalent acyl-enzyme intermediate is generated and the substrate is an acyl donor. The intermediate is then hydrolyzed by the nucleophilic attack of an activated water molecule. In the presence of relatively high concentrations of primary amine, which are not achieved under physiological conditions, nucleophilic attack by an amino group instead of a water molecule forms an amide bond (Fig. 1) [6–11]. In this reaction, termed aminolysis, the primary amine acts as an acyl acceptor. Because amino acids can act as acyl acceptors, the unnatural aminolysis reaction of serine peptidases has attracted attention as a method for synthesizing various peptides that cannot be produced under natural conditions.

Several enzymes in the MEROPS peptidase database belonging to the S12 family, which have a catalytic Ser/Lys dyad, exhibit high aminolysis activity for various types of substrates such as amides esters and peptides [12–14]. Four crystal structures of S12 family peptidases have been reported: D-Ala-D-Ala carboxypeptidase B (D,D-peptidase), class C β -lactamase, D-amino acid amidase (DAA) and D-stereospecific aminopeptidase [15–18]. D,D-Peptidase and D-stereospecific aminopeptidase catalyze peptide bond formation by their aminolysis activity [12–14]. Based on these crystal structures, the structural factors responsible for the substrate specificities have been identified [19]. However,

their substrate specificities and the mechanism for recognizing acyl acceptors for the aminolysis reaction are not fully understood.

Recently, we found a new serine peptidase, D-stereospecific amidohydrolase (DAH), in *Streptomyces* sp. 82F2. The enzyme belongs to the S12 peptidase family and has high aminolysis activity in addition to hydrolyzing various D-aminoacyl and D,D-configuration dipeptide derivatives [20]. In the DAH aminolysis reaction, the enzyme preferentially uses D-aminoacyl derivatives as acyl donors and L-amino acids and their derivatives as acyl acceptors, producing dipeptides with a DL-configuration [21]. Therefore, the enzyme is of particular interest for synthesizing various peptides incorporating D-amino acids. DAH has been used to synthesize a cyclic dipeptide that inhibits family 18 chitinase, cyclo (D-Pro-L-Arg) in a one-step/one-pot reaction.

In the present study, we showed that DAH can use 1,8-diaminooctane and other amino compounds as acyl acceptors in the aminolysis reaction. We crystallized this enzyme in the presence of 1,8-diaminooctane and the crystal structure of the DAH complex with 1,8-diaminooctane was obtained at a resolution of 1.49 Å. Comparative analysis with homologous enzymes provided insights into structural factors for the substrate specificity and aminolysis of DAH.

Results and Discussion

Diamino-alkane acts as an acyl acceptor substrate

First, we assessed the effect of 1,8-diaminooctane on the catalytic function of DAH. The *p*-nitroaniline release activity of DAH for D-Phe-*p*-nitroanilide (pNA) is accompanied by the acyl-enzyme intermediate formation (Fig. 2A). The intermediate is then deacylated by the nucleophilic attack of activated water to form D-Phe (Fig. 3A). If the amino group of 1,8-diaminooctane attacks the acyl-DAH intermediate instead

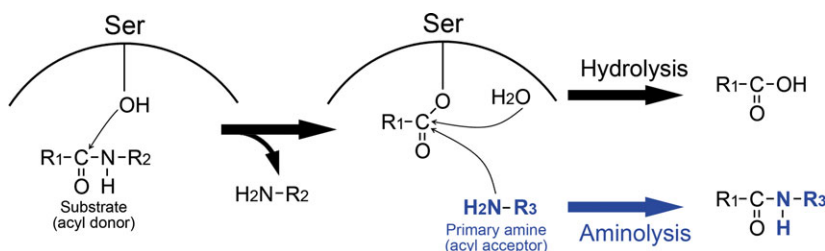


Fig. 1. Scheme of the hydrolysis and aminolysis reactions catalyzed by serine peptidases.

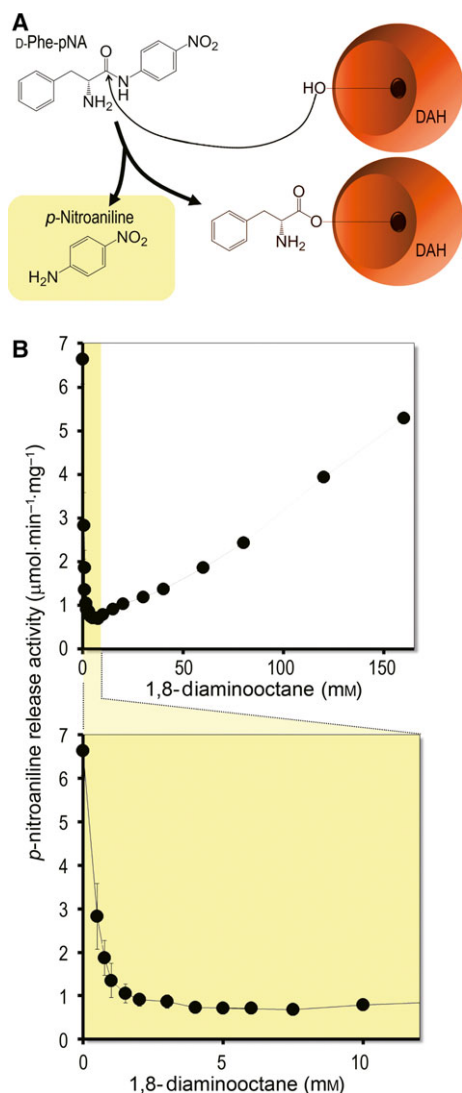


Fig. 2. Effect of 1,8-diaminooctane on acyl-enzyme intermediate formation of DAH. (A) Reaction scheme of the formation of the acyl-enzyme intermediate. *p*-Nitroaniline is a product of the formation of the acyl-enzyme intermediate when the D-Phe-pNA substrate is used. (B) Effect of 1,8-diaminooctane on the acyl-enzyme intermediate formation. The release of *p*-nitroaniline from D-Phe-pNA associated with the acyl-enzyme intermediate formation was measured every minute. Each value represents the mean \pm SD of values from four independent experiments.

of a water molecule, (*R*)-2-amino-*N*-(8-aminoethyl)-3-phenylpropanamide (D-Phe-1,8-diaminooctane) should be formed (Fig. 3A).

As shown in Fig. 2B, the release of *p*-nitroaniline by DAH (acyl-enzyme intermediate formation) decreased as the 1,8-diaminooctane concentration increased to \sim 5 mM. However, in the presence of more than 10 mM 1,8-diaminooctane, *p*-nitroaniline release by DAH gradually increased with the 1,8-diaminooctane

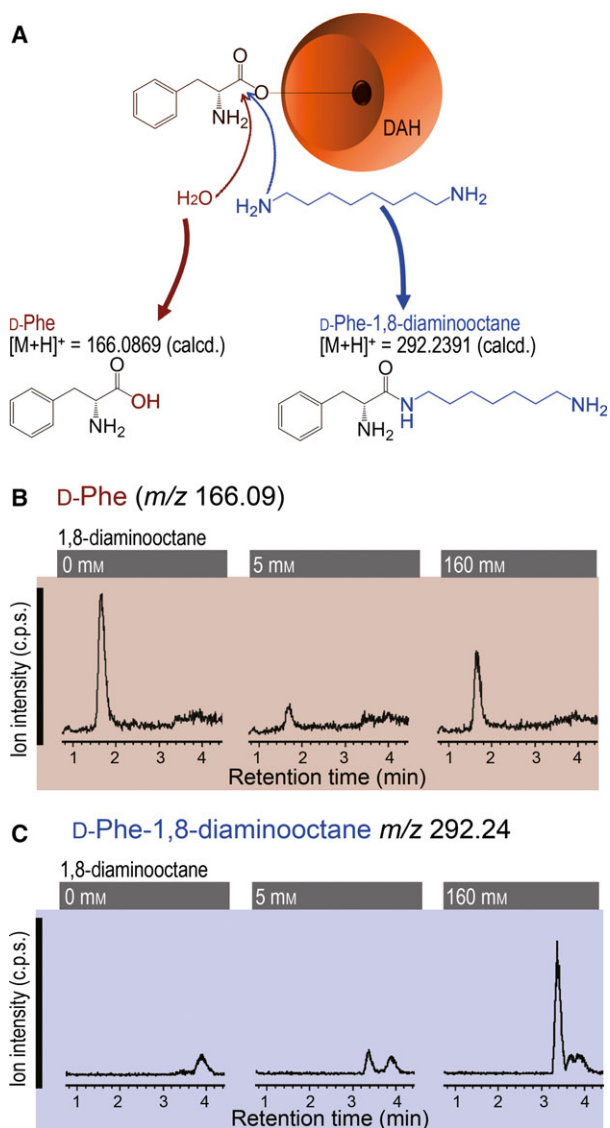


Fig. 3. Effect of 1,8-diaminooctane on the hydrolysis and aminolysis reactions catalyzed by DAH. (A) Reaction scheme after the formation of the acyl-enzyme intermediate when D-Phe-pNA was used a substrate. D-Phe is the product of the nucleophilic attack of water on the carbonyl carbon of the acyl-enzyme intermediate. By contrast, 1,8-diaminooctane attacks the acyl-enzyme intermediate to produce D-Phe-1,8-diaminooctane. (B, C) Extracted ion chromatograms of the products of the DAH reaction, D-Phe and D-Phe-1,8-diaminooctane, using 0.8 mM D-Phe-pNA for 120 min. Mass spectra data: D-Phe, calculated for $C_9H_{11}NO_2$ $[M+H]^+$: 166.0869, found: 166.0851–166.0882. D-Phe-1,8-diaminooctane, calculated for $C_{17}H_{29}N_3O$ $[M+H]^+$: 292.2391, found: 292.2385–292.2413.

concentration (Fig. 2B). These results indicate that 1,8-diaminooctane up to a concentration of \sim 5 mM inhibits acyl-enzyme intermediate formation, whereas higher 1,8-diaminooctane concentrations rescue the acyl-enzyme intermediate formation.

Next, we examined the reaction after the acyl-enzyme intermediate formation. Figure 3B shows that the production of D-Phe, which is a hydrolysis product of the acyl-enzyme intermediate, was retarded in the presence of 5 mM 1,8-diaminooctane, which is consistent with the observation that up to ~5 mM 1,8-diaminooctane suppressed the acyl-enzyme intermediate formation (Fig. 2B). The addition of 160 mM 1,8-diaminooctane increased the formation of D-Phe, which is also consistent with the excess of 1,8-diaminooctane rescuing *p*-nitroaniline formation. Although acyl-enzyme intermediate formation is retarded by up to 5 mM 1,8-diaminooctane, D-Phe-1,8-diaminooctane, which is produced by aminolysis of the intermediate by 1,8-diaminooctane, was detected under the same conditions. Further addition of 1,8-diaminooctane markedly increased the aminolysis reaction (Fig. 3C). Because 160 mM 1,8-diaminooctane rescued acyl-enzyme intermediate formation, D-Phe formation was also slightly rescued. These observations of the acyl-intermediate formation and deacylation of the intermediate suggest that acyl-enzyme intermediate formation was facilitated by the presence of a large

amount of 1,8-diaminooctane. The increased amount of acyl-enzyme intermediate was competitively consumed by deacylation with a water molecule and aminolysis with 1,8-diaminooctane.

The addition of 1,8-diaminooctane, other alkylamines, amino alcohols and L-amino acids to the enzyme reaction mixture also results in an aminolysis reaction (Table 1), indicating that DAH recognizes these amine compounds as acyl acceptor substrates. By contrast, DAH did not recognize D-amino acids, secondary and tertiary amine compounds and some amines, including Tris and amino sugars, as acyl acceptor substrates (data not shown).

Next, we investigated the enzyme kinetics of the aminolysis reaction with several acyl donor and acceptor substrates. The K_m value for D-Phe-pNA could not be determined because of its low solubility (< 0.9 mM at pH 8.5). Therefore, D-Phe-benzyl ester (OBzl) and 1,8-diaminooctane were used as acyl donor and acceptor substrates, respectively. The K_m value for D-Phe-OBzl hydrolysis (0.036 mM) was determined in a previous study [21]. As shown in Table 2, the apparent K_m values for D-Phe-OBzl and 1,8-diaminooctane for

Table 1. Recognition of amine compounds as acyl acceptor substrates for aminolysis. Recognition of the acyl acceptor was evaluated by UPLC ESI-TOF-MS after the enzyme reaction with 20 mM D-Phe-OBzl, 200 mM additive and 0.2 M Tris-HCl (pH 8.5). Mass spectra data of the D-phenylalanyl derivatives are listed.

Chemicals	Recognition as acyl acceptor	Aminolysis product (formula)	Calculated [M + H] ⁺	Observed
1,3-Diaminopropane	± ^a	D-phenylalanyl 1,3-diaminopropane (C ₁₂ H ₁₉ N ₃ O)	222.1608	222.1648
1,4-Diaminobutane	+	D-phenylalanyl 1,4-diaminobutane, (C ₁₃ H ₂₁ N ₃ O)	236.1765	236.1794
1,5-Diaminopentane	+	D-phenylalanyl 1,5-diaminopentane (C ₁₄ H ₂₃ N ₃ O)	250.1921	250.1930
1,6-Diaminohexane	+	D-phenylalanyl 1,6-diaminohexane (C ₁₅ H ₂₅ N ₃ O)	264.2078	264.2054
1,7-Diaminoheptane	+	D-phenylalanyl 1,7-diaminoheptane (C ₁₆ H ₂₇ N ₃ O)	278.2234	278.2271
1,8-Diaminooctane	+	D-phenylalanyl 1,8-diaminooctane (C ₁₇ H ₂₉ N ₃ O)	292.2391	292.2397
1,10-Diaminodecane	+	D-phenylalanyl 1,10-diaminodecane (C ₁₉ H ₃₃ N ₃ O)	320.2704	320.2705
Ethylamine	± ^a	D-phenylalanyl ethylamine (C ₁₁ H ₁₆ N ₂ O)	193.1342	193.1342
Propylamine	+	D-phenylalanyl propylamine (C ₁₂ H ₁₈ N ₂ O)	207.1499	207.1500
Isopropylamine	– ^b			
Butylamine	+	D-phenylalanyl butylamine (C ₁₃ H ₂₀ N ₂ O)	221.1655	221.1687
Hexylamine	+	D-phenylalanyl hexylamine (C ₁₅ H ₂₄ N ₂ O)	249.1969	249.1959
1-Aminodecane	+	D-phenylalanyl 1-aminodecane (C ₁₉ H ₃₂ N ₂ O)	305.2595	305.2599
2-Aminoethanol	± ^a	D-phenylalanyl 2-aminoethanol (C ₁₁ H ₁₆ N ₂ O ₂)	209.1291	209.1286
4-Amino-1-butanol	+	D-phenylalanyl 4-amino-1-butanol (C ₁₃ H ₂₀ N ₂ O ₂)	237.1604	237.1635
6-Amino-1-hexanol	+	D-phenylalanyl 6-amino-1-hexanol (C ₁₅ H ₂₄ N ₂ O ₂)	265.1918	265.1917
10-Amino-1-decanol	+	D-phenylalanyl 10-amino-1-decanol (C ₁₅ H ₂₄ N ₂ O ₂)	321.2544	321.2547
Gly	+ ^c	D-Phe-Gly		
L-Ala	+ ^c	D-Phe-L-Ala		
L-Lys	+ ^c	D-Phe-L-Lys		
L-Leu	+ ^c	D-Phe-L-Leu		
L-Trp	+ ^c	D-Phe-L-Trp		

^a ±, Low amount of product.

^b –, Not detectable.

^c +, Refer to Arima *et al.* [21].

Table 2. K_m values of DAH for hydrolysis and amide bond formation activity. K_m values were calculated from a nonlinear regression fit to the Michaelis–Menten equation using initial estimates from double-reciprocal plots.

Reaction	Substrate	K_m (mM)
D-Phe-OBzl hydrolysis	D-Phe-OBzl	0.036 ^a
D-Phe-1,8-diaminooctane synthesis	D-Phe-OBzl	14.3
	1,8-Diaminooctane	626

^a Value given in Kato *et al.* [13].

D-Phe-1,8-diaminooctane synthesis were 14.3 and 626 mM, respectively. The substantially larger D-Phe-OBzl K_m value for aminolysis than for hydrolysis implies that 1,8-diaminooctane inhibits D-Phe-OBzl binding to the enzyme.

Structure of DAH

Because 1,8-diaminooctane and other compounds containing an amino group accept an acyl group and undergo aminolysis by DAH, we crystallized DAH in the presence of amino compounds. The addition of 3% 1,8-diaminooctane to DAH produced pyramidal crystals. Although several types of crystals were obtained in the presence of alkylamines (data not shown), the quality of these crystals was mostly poor. We determined the crystal structure of DAH at a resolution of 1.49 Å using the pyramidal crystals.

The overall structure of the enzyme is presented in Fig. 4A. The enzyme consists of α -rich and β -rich regions. The β -rich region is formed by residues 38–86 and 224–379, and consists of six main antiparallel β -strands flanked by four α -helices. The α -helix rich region (residues 87–223) includes another 11 α -helices (Fig. 4A).

There are two motifs, Ser-x-x-Lys and Tyr-x-Asn, which are necessary for the expression of the enzyme activity [15,22] in the N-terminal (Ser86–Lys89) and the internal region (Tyr191–Asn193) of DAH, respectively (Fig. 5). Crystallographic analysis of the enzyme revealed that DAH possesses a large cavity that leads to the catalytic center. The side chains of Ser86 and Lys89 that create a catalytic Ser/Lys dyad in S12 family peptidases [15] were positioned at the center of the large cavity (Fig. 4B). Tyr191, which is close to the Ser/Lys dyad, acts as the general base to activate Ser as a nucleophile for the acyl donor during the acylation step and the water molecule during hydrolysis [22–24]. In addition, there is a small pocket close to the catalytic center of Ser86, Ly89 and Tyr191 (Fig. 4B).

In the structure of the catalytic center of DAH, Ser86 O^γ forms a hydrogen bond with the backbone amide of Gly337, which makes the hydroxyl group point further away from Lys89. Lys89 N^ε forms hydrogen bonds with Tyr 191 O^η, Asn193 O^δ and the backbone carbonyl oxygen of Ala270 (Fig. 4C). The interaction decreases the pK_a of general base Tyr to form a phenolate anion that activates the nucleophilic Ser [23,24].

Substantially elongated electron densities in the $F_o - F_c$ and $2F_o - F_c$ simulated annealing omit maps were observed at the entrance of the active site pocket (Fig. 4D). The length of this electron density is comparable to 1,8-diaminooctane, which is contained in the crystallization solution, and no other compounds are consistent with this electron density shape. Therefore, we assigned this electron density as 1,8-diaminooctane. The distance between the active site Ser residue and the bound 1,8-diaminooctane molecule was 7.3 Å (Fig. 4E). The binding model shows that the amino group of 1,8-diaminooctane forms hydrogen bonds with the backbone carbonyl of Phe155 and a water molecule that is hydrogen bonded to another water molecule and Asp362 O^δ. The other amino group of 1,8-diaminooctane forms a hydrogen bond with Ser342 O^γ (Fig. 4D). In addition, Phe155 is involved in a hydrophobic interaction with the alkyl chain of 1,8-diaminooctane. We also found another elongated $F_o - F_c$ simulated annealing omit map close to the active site. This is another potential 1,8-diaminooctane binding site because the shape of the $F_o - F_c$ electron density is similar to that for the other binding site. In addition, one end of the density is close to the Ser367 and Ser343 side chains, which enable hydrogen-bonding interactions with the diamine. However, because the $2F_o - F_c$ simulated annealing omit map is poor, probably as a result of low affinity and low occupancy, the diamine cannot be assigned unambiguously, and thus only the diamine bound to the former binding site was included in the final stage of the refinement.

Selectivity of substrate length and bulkiness

DAH prefers D-aminoacyl derivatives and D,D-configuration dipeptide derivatives with large, hydrophobic side chains as acyl donors [20,21]. By contrast to DAH, D,D-peptidase and DAA recognize the C-terminal D-Ala of oligopeptides and D-aminoacyl amides with bulky hydrophobic side chains, respectively, as acyl donors. Structural comparison of these enzymes with DAH revealed that the overall structure of DAH is analogous to D,D-peptidase and DAA (rmsd values:

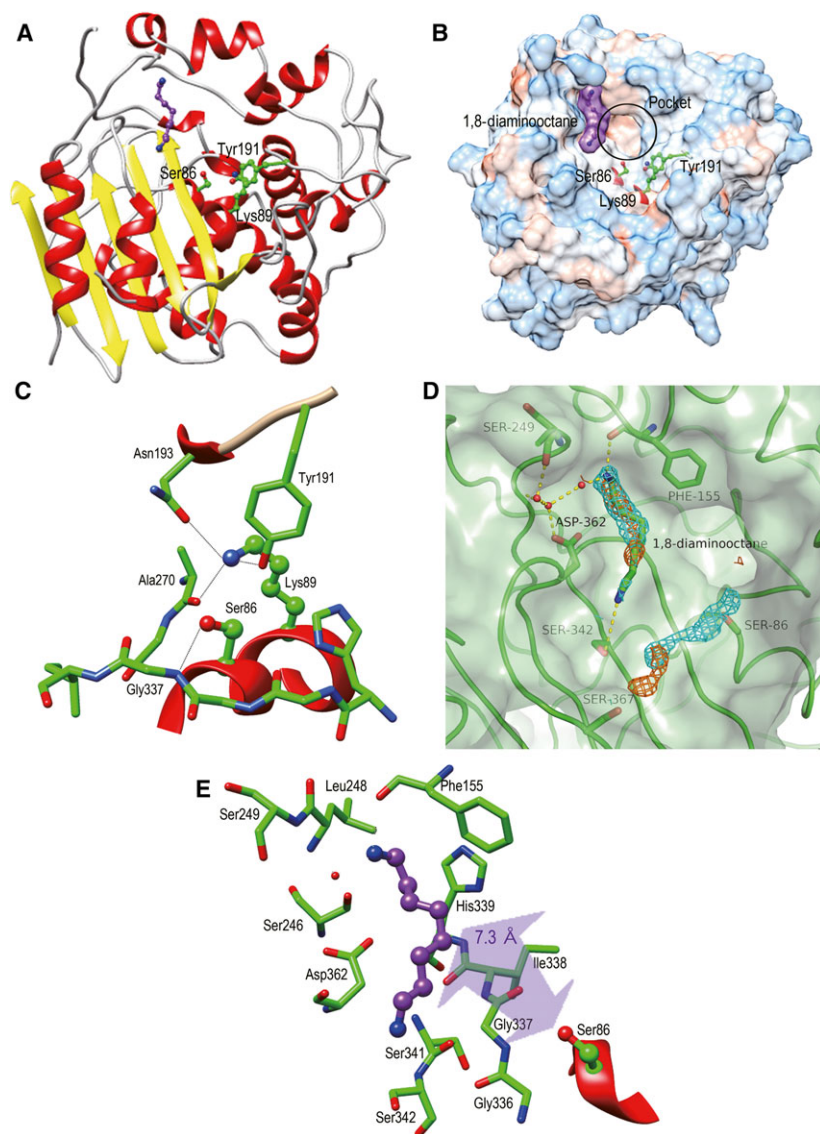


Fig. 4. Overall structure and local structure around the active site Ser of DAH. (A) Overall structure of DAH that interacts with 1,8-diaminooctane. α -Helices and β sheets are shown in red and yellow, respectively. The bound 1,8-diaminooctane and active site residues (Ser86, Lys89 and Tyr191) are shown as a purple and green ball and stick models, respectively. (B) Surface model of DAH. The bound 1,8-diaminooctane and active site residues (Ser86, Lys89 and Tyr191) are shown as a purple and green ball and stick model, respectively. (C) Residues surrounding the active site Ser86 and Lys89. Ser86 and Lys89 are shown as a ball and stick model according to the atom type. Other residues are shown as sticks colored according to the atom type. Hydrogen bonds are represented as broken lines. (D) $F_o - F_c$ and $2F_o - F_c$ simulated annealing omit electron density maps (countered at 3.0 and 1.0 σ , respectively) are shown as cyan and orange meshes, respectively. The length of this electron density is comparable to 1,8-diaminooctane. Hydrogen bonds are represented as broken lines. (E) Residues surrounding the bound 1,8-diaminooctane. Carbon and nitrogen atoms of the bound 1,8-diaminooctane are purple and blue, respectively. Residues are shown as sticks colored according to the atom type.

1.5 and 2.3 Å for D,D-peptidase and DAA, respectively) (Fig. 6, left). Of these enzymes, DAH possesses the largest cavity leading to the catalytic center (Fig. 6, middle). DAH and DAA have a larger pocket at the bottom of the cavity than D,D-peptidase (Fig. 6, right).

Previous studies of D,D-peptidase and DAA have shown that the large D,D-peptidase cavity accommodates the peptide substrate, and the narrow space in the DAA cavity limits the length of the substrate [17,25,26]. By contrast, the DAA active site pocket is larger than that of D,D-peptidase (Fig. 6B,C, right). The larger active site pocket of DAA can recognize and accommodate D-aminoacyl amides with bulky side chains. The crystal structure of DAA complexed with D-Phe reveals that the ligand fits snugly in the DAA active site pocket, as described below. In DAH

(Fig. 6A), the enzyme has a large cavity and active site pocket. Therefore, the large cavity in DAH allows the peptide substrate to enter, and the large space in the active site pocket accommodates the large side chain of the acyl donor substrate.

Structural factors for recognizing the substrate N-terminal amino acid

Among DAH, D,D-peptidase, and DAA, only D,D-peptidase exhibits carboxypeptidase activity. The structure of D,D-peptidase complexed with a peptideglycan mimic, β -sultam, suggests that Arg285 recognizes the terminal carboxylate of the peptide substrate and expresses the carboxypeptidase activity [27]. The terminal carboxylate recognition by the Arg residue is also

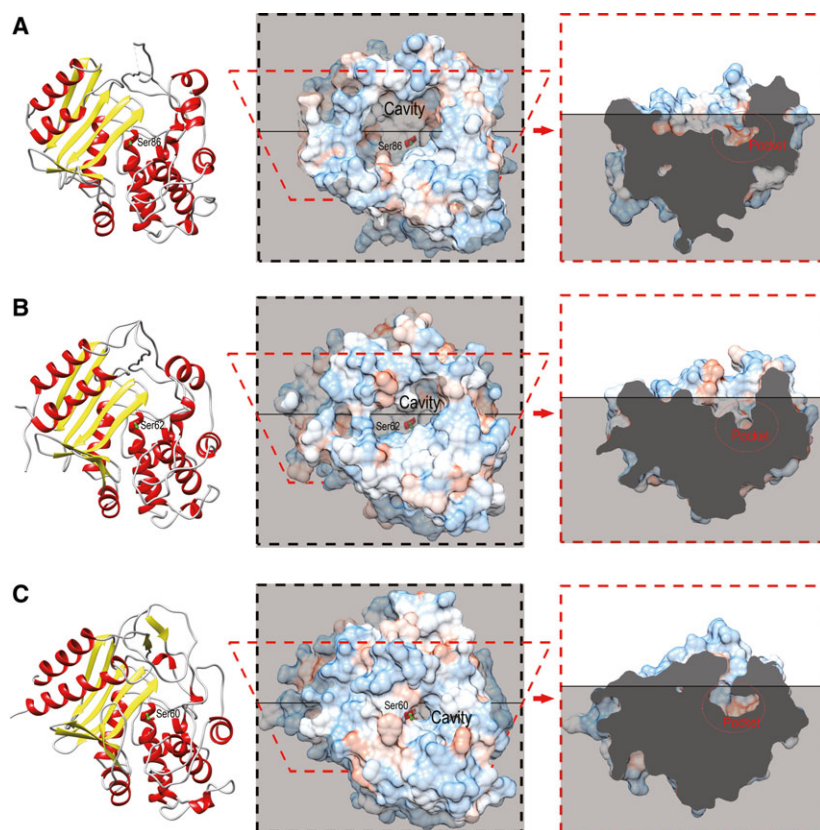


Fig. 6. Comparison of the folds and cavity shapes of (A) DAH, (B) D,D-peptidase (Protein Data Bank code: [3PTE](#)) [15] and (C) DAA (Protein Data Bank code: [2EFX](#)) [17]. Corresponding ribbon models are shown on the left with α -helices and β sheets in red and yellow, respectively. Active site Ser residues of the enzymes are shown as ball and stick models colored according to the atom type. The hydrophobic surfaces are also shown (middle). Active site Ser residues of the enzymes are shown as ball and stick models colored according to the atom type. Corresponding cross-sectional views are shown on the right. The structures of respective enzymes are superimposed on the model of DAH, and then the cross-sectional view of respective enzymes with the same angle is created. The enzyme molecules are shown as hydrophobic surfaces.

aminolysis in the presence of 1,8-diaminooctane. The crystal structures of 1,8-diaminooctane-bound DAH and an inhibitor-bound D,D-peptidase provide a scenario that explains these observations. The crystal structure of DAH revealed that the active site pocket of this enzyme is narrowed by the diamine, and thereby the entry of the acyl donor is inhibited by the presence of 1,8-diaminooctane. The $F_o - F_c$ simulated annealing omit electron density map implies that the diamine could bind to the second site, which is close to the active site Ser. The diffuse $2F_o - F_c$ electron density of the second site suggests that the affinity for the diamine is relatively low. It has been reported that D,D-peptidase is completely inhibited by a peptidoglycan mimic [34]. The peptidoglycan mimic covers the active site pocket, and thus the ligand completely blocks the access of the acyl donor to the active site Ser. Comparing 1,8-diaminooctane-bound DAH with D,D-peptidase inhibited by the peptidoglycan mimic indicated that 1,8-diaminooctane overlaps with the Gly-L-diaminopimelic acid moiety of the peptideglycan mimic. However, the active site pocket and the Ser86 side chain in DAH are accessible for an acyl donor, even when the potential second diamine binding site is occupied by 1,8-diaminooctane, unlike the peptidoglycan mimic-bound D,D-peptidase. Therefore, the crystal-

lographic data can explain the partial inhibition of acylation of the enzyme. Aminolysis, which is deacylation of the acyl-enzyme intermediate by the diamine, is hindered by very high concentrations of water (> 5500 mM), which consumes the acyl-enzyme intermediate by hydrolysis. Addition of a large amount of 1,8-diaminooctane leads to the deacylation of the acyl-enzyme intermediate by the diamine, which is probably located close to the enzyme-bound acyl group and Ser86. The increased deacylation rescues acyl-enzyme intermediate formation and the intermediate is competitively attacked by water molecules and the diamine. The 1,8-diaminooctane in the crystal structure is unlikely to act as an acyl acceptor because the amino groups of 1,8-diaminooctane are too far (12.8 and 8.0 Å) from the active site Ser O γ . Based on the crystal structure, it is difficult to identify unambiguously the diamine binding site where 1,8-diaminooctane binds and attacks the acyl-enzyme intermediate during aminolysis. However, there is a possible binding site that probably has lower affinity for the diamine close to the second diamine binding site (Fig. 7C,D). If 1,8-diaminooctane bound to the second site, one of the diamine amino groups would form a hydrogen bond with Ser367 and/or Ser343, pointing the other amino group toward the acyl group of the intermediate,

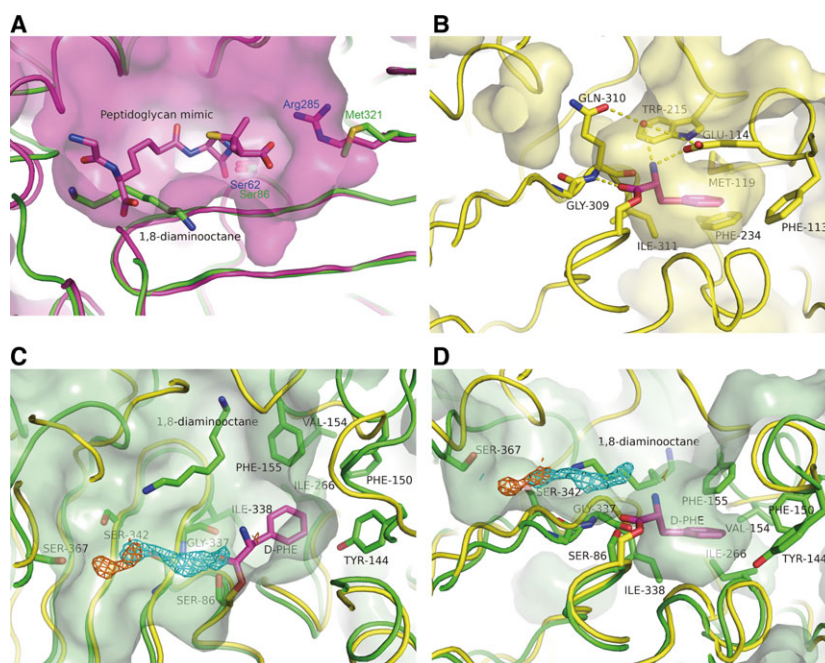


Fig. 7. Comparison of the active sites of DAH, D,D-peptidase and DAA. (A) Superimposed ligand binding modes of DAH and D,D-peptidase. The main chains of D,D-peptidase binding a peptidoglycan mimic (Protein data bank code: [1PW1](#)) [34] and 1,8-diaminooctane-bound DAH are shown as magenta and green loop models, respectively. The DAH ligand, 1,8-diaminooctane, and the D,D-peptidase peptide glycan mimic ligand are shown as stick models. The molecular surface of D,D-peptidase is shown as magenta transparent surface. (B) Active site structure of D-Phe-bound DAA. Main chain and side chain carbon atoms of DAA binding D-Phe (Protein data bank code: [2DNS](#)) [17]. The DAA ligand, D-Phe, is shown in magenta. The molecular surface of DAA is shown as a yellow transparent surface. (C) Overlaid active site structures of DAH and D-Phe-bound DAA. Main chain and side chain carbon atoms of DAH are shown in green. $F_o - F_c$ and $2F_o - F_c$ simulated annealing omit electron density maps (countered at 3.0 and 1.0 σ , respectively) are shown as cyan and orange meshes, respectively. The molecular surface of DAH is shown as a light green transparent surface. (D) Superimposed active site structures of DAH and DAA as shown in (C) viewed from different angle.

allowing the diamine to attack. Although DAH can use L-amino acids as acyl acceptors, free D-amino acids are very poor acyl acceptors for DAH. Therefore, both the acyl group at the active site and the enzyme surface around the acyl group would be required for proper binding of 1,8-diaminooctane to accept the acyl group. To clarify the recognition mechanisms for the acyl acceptor in DAH aminolysis, further crystallographic studies are required, such as crystallization of DAH bound to a stable acyl group analogue in the presence of 1,8-diaminooctane.

Conclusions

We solved the crystal structure of DAH complexed with 1,8-diaminooctane. The overall enzyme structure is analogous to D,D-peptidase and DAA. Comparing the structures indicated that DAH possesses the largest cavity leading to the catalytic center. By contrast, the arrangement of the residues in the active site pocket is similar to that of DAA complexed with D-Phe. In addition, the residue corresponding to Arg285 of

D,D-peptidase, which is expected to be necessary for the carboxypeptidase activity as shown by a previous mutagenesis study, is replaced by Met321 in DAH. This structural feature is probably responsible for the substrate specificity of DAH. Because 1,8-diaminooctane inhibits acyl-enzyme intermediate formation, the 1,8-diaminooctane-bound DAH structure can explain the inhibition mode of intermediate formation. The excess 1,8-diaminooctane acts as an acyl acceptor substrate in DAH aminolysis. Although we identified a potential binding mode of the diamine that attacks the acyl-enzyme intermediate, the exact location of the diamine binding site for aminolysis should be determined by X-ray crystallography to shed further light on the aminolysis mechanism.

Materials and methods

Expression and purification

We cultivated *Escherichia coli* Rosetta (DE3) harboring the expression vector for DAH from *Streptomyces* sp. 82F2,

pET-82F2DAP [21] at 25 °C for 48 h in Overnight Expression Instant TB medium (50 mL; Novagen Inc., Madison, WI, USA) in 10 test tubes (5 mL of medium in each tube). The culture was centrifuged to remove the cells, and the recombinant enzyme was purified. The culture supernatant was dialyzed against 20 mM sodium acetate (pH 5.5). The dialysate was loaded onto a spin column (Vivapure-S; Sartorius, Gottingen, Germany) equilibrated with 20 mM sodium acetate (pH 5.5). The bound protein was washed with sodium acetate buffer containing 0.1 M NaCl, and eluted with sodium acetate buffer containing 0.4 M NaCl. The eluate was pooled and dialyzed against 20 mM Tris-HCl (pH 8.0) containing 0.5 M NaCl. Then, it was concentrated to more than 10 mg⁻¹·mL⁻¹ with a centrifugal filter (Amicon Ultra; Millipore Corp., Billerica, MA, USA). The homogeneity of the purified proteins was confirmed by 12% SDS/PAGE under denaturing conditions [35].

Crystallization

DAH crystals were grown at 20 °C through sitting drop vapor diffusion by mixing a protein solution (17 mg·mL⁻¹ protein in 20 mM Tris-HCl, pH 8.0, with 0.5 M NaCl) and a reservoir solution (1.5 M citrate, pH 6.0). Although several types of crystals were obtained in the presence of alkylamines (3% 1,6-diaminohexane, 1,7-diaminoheptane, and 6-amino-1-hexanol) during additive screening, the quality of these crystals was mostly poor. Only the pyramidal crystals obtained in the presence of 1,8-diaminooctane were of sufficient quality for diffraction experiments.

Data collection and structure determination

The crystals were harvested in solution containing 1.5 M citrate (pH 6.0), 3% diamino-alkane and 20% glycerol, and were flash-cooled in a nitrogen stream at 100 K. DAH crystallized in the $P2_12_12_1$ space group, with unit cell dimensions: $a = 59.29$ Å, $b = 74.68$ Å and $c = 76.45$ Å.

Diffraction data was collected at SPring-8 BL26B1 (Hyogo, Japan). The data were indexed, scaled, merged and reduced with HKL2000 [36] and IMOSFLM packages [37]. The initial phases were obtained by molecular replacement with PHASER [38] using the structure of D,D-peptidase (Protein data bank code: [1CEF](#); 37% sequence identity) as a search model.

The structure was refined by PHENIX [39] against 1.5 Å diffraction data. The final atomic model contained 341 amino acid residues. The data collection and refinement statistics for the crystal structure of DAH are presented in Table 3. The asymmetric unit contained one protomer. The $F_o - F_c$ and $2F_o - F_c$ simulated annealing omit maps suggested that a long ligand bound at the entrance of the active site pocket. Thus, 1,8-diaminooctane was fitted into the elongated electron density in the structural model. We

Table 3. Data collection and refinement statistics for the crystal structure of DAH. $R_{\text{merge}} = \sum(|I_i - \langle I \rangle|) / \sum I_i$, where I_i is the intensity of an observation, and $\langle I \rangle$ is the mean value for that reflection, and summations are over all reflections. $R_{\text{factor}} = \sum |F_o - F_c| / \sum F_o$, where F_o and F_c are the observed and calculated structure factors, respectively. R_{free} factor was calculated with 5% of the data.

Crystal cell parameter and data collection	
Unit cell parameter	
a, b, c (Å)	59.29, 74.68, 76.45
Space group	$P2_12_12_1$
Relative molecular mass	37 394
Matthews coefficient (Å ³ /Da)	2.26
Solvent content (%)	45.7
Collection and reduction	
Wavelength (Å)	1.000
Resolution limit (Å)	1.49
Number of total reflections	321 232
Number of unique reflections	54 051
Completeness (%)	96.3 (75.2) ^a
I/σ	20.0 (3.68) ^a
R_{merge} (%)	5.3 (24.4) ^a
$CC_{1/2}$	0.990 (0.928) ^a
Wilson B -factor (Å ²)	14.9
Refinement	
Resolution range (Å)	29.5–1.49
R_{work} (%)	14.1
R_{free} (%)	16.2
rmsd (bond length) (Å)	0.009
rmsd (bond angle) (°)	1.32
Number of protein residues	340 of 349
Chemical component	1,8-diaminooctane
Average B -factor (Å ²)	
All atoms	17.4
Protein atoms	15.4
1,8-diaminooctane	31.4
Ramachandran plot ^b	
Favored (%)	97.3
Allowed (%)	2.1
Outliers (%)	0.6

^a Values in parenthesis are for the highest resolution shell.

^b Ramachandran plot was calculated using MOLPROBITY [41].

also observed another elongated $2F_o - F_c$ simulated annealing omit map close to the active site. Because the shape of this density is similar to that of the other binding site, this is another potential 1,8-diaminooctane binding site. However, the $2F_o - F_c$ simulated annealing omit maps of this site is weak, probably as a result of the low affinity and low occupancy of the ligand. Thus, we did not add the second 1,8-diaminooctane to the structural model. A final round of refinement was performed using a model with only one 1,8-diaminooctane molecule. Coordinates and structure factors for DAH have been deposited in the Protein Data Bank at the Research Collaboratory for Structural Bioinformatics under code [3WWX](#). Figures 4–6 were

prepared using UCSF CHIMERA [40] and PYMOL (The PyMOL Molecular Graphics System, Version 1.7.4; Schrödinger, LLC, New York, NY, USA).

Effect of 1,8-diaminooctane on the acyl-enzyme intermediate formation

The effect of the 1,8-diaminooctane concentration on the acyl-enzyme intermediate formation of DAH was investigated by a continuous spectrophotometric assay with 0.8 mM D-Phe-pNA as the substrate. In the assay, DAH (5 μ L, 100 μ g·mL⁻¹) was incubated with a mixture containing 0.3 M Tris-HCl (75 μ L, pH 8.5) and various concentrations of 1,8-diaminooctane (5–160 mM) for 120 min at 25 °C, followed by the addition of 4 mM D-Phe-pNA (20 μ L). The increased in A_{405} caused by the release of *p*-nitroaniline associated with the acyl-enzyme intermediate formation was monitored continuously and measured every minute using a Microtiter plate reader (680; Bio-Rad Laboratories Inc., Hercules, CA, USA). The initial activity rate was determined from a linear part of the optical density profile of *p*-nitroaniline measured with the same instrument.

Aminolysis reaction using a diamino-alkane as an acyl acceptor

An aminolysis reaction using a diamino-alkane as an acyl acceptor was performed. 0.5 M D-Phe-OBzl (2 μ L) dissolved in dimethyl sulfoxide and 0.5 M diamino-alkane (20 μ L) were added to 0.5 M Tris-HCl (26 μ L, pH 8.5). The reaction was initiated by adding 0.2 mg·mL⁻¹ DAH solution (2 μ L) to the mixture. The reaction was continued at 4 °C for 4 h, and was terminated by adding 0.5 M HCl (50 μ L) to the mixture. The reaction mixture was analyzed by MS.

To determine the apparent K_m value for D-Phe-OBzl for D-Phe-1,8-diaminooctane synthesis, the enzyme reaction was conducted at different D-Phe-OBzl concentrations (5–15 mM) in the presence of 0.2 M 1,8-diaminooctane at 4 °C and pH 8.5 for 5 min. To determine the apparent K_m value for 1,8-diaminooctane for D-Phe-1,8-diaminooctane synthesis, the enzyme reaction was performed at different 1,8-diaminooctane concentrations (50–150 mM) in the presence of 20 mM D-Phe-OBz at 4 °C and pH 8.5 for 5 min.

MS analysis

The molecular mass of the aminolysis reaction products was determined by ultra-performance liquid chromatography (UPLC)-ESI-TOF MS equipped with a C18 reverse-phase system. For UPLC-ESI-TOF MS analysis, the reaction mixture was diluted by 1000-fold v/v with 0.1% formic acid. After the solution was filtered, aliquots of each sample (5 μ L) were analyzed by UPLC-ESI-TOF MS (LCT

Premier XE; Waters Corp., Milford, MA, USA). Each sample was eluted with solvent A–solvent B 95 : 5 for 2 min, solvent A–solvent B 80 : 20 for 1 min, solvent A–solvent B gradient of 80 : 20 to 50 : 50 for 2 min, and solvent A–solvent B of 20 : 80 for 2 min. Solvent A was Milli-Q water containing 0.1% formic acid and solvent B was acetonitrile containing 0.1% formic acid. Data were processed using MASSLYNX (Waters Corp.).

Acknowledgements

This work was supported in part by a Grant-in-Aid for Scientific Research (C) from the Japan Society for the Promotion of Science to J.A. (No. 26450124). The evaluation of the acyl acceptor substrate was supported by the Naito Foundation through funding to J.A.

Author contributions

J.A. and S.N. planned the project. J.A. performed experiments depicted in Figs 1, 2, and 3. K.S. and K.M. performed the purification and crystallization of DAH. Y.T. contributed experiments depicted in Table 1. Y.I. contributed experiments depicted in Table 2. T.H. and S.N. determined the crystal structure of DAH. J.A. and S.N. wrote the paper. All authors discussed the results and commented on the manuscript.

References

- 1 Rawlings ND, Waller M, Barrett AJ & Bateman A (2014) MEROPS: the database of proteolytic enzymes, their substrates and inhibitors. *Nucleic Acids Res* **42**, D503–D509.
- 2 Dodson G & Wlodawer A (1998) Catalytic triads and their relatives. *Trends Biochem Sci* **23**, 347–352.
- 3 Shin S, Yun YS, Koo HM, Kim YS, Choi KY & Oh BH (2003) Characterization of a novel Ser-cisSer-Lys catalytic triad in comparison with the classical Ser-His-Asp triad. *J Biol Chem* **278**, 24937–24943.
- 4 Paetzel M & Strynadka NC (1999) Common protein architecture and binding sites in proteases utilizing a Ser/Lys dyad mechanism. *Protein Sci* **8**, 2533–2536.
- 5 Paetzel M & Dalbey RE (1997) Catalytic hydroxyl/amine dyads with serine proteases. *Trends Biochem Sci* **22**, 28–31.
- 6 Bratovanova EK & Petkov DD (1987) Glycine flanked by hydrophobic bulky amino acid residues as minimal sequence for effective subtilisin catalysis. *Biochem J* **248**, 957–960.
- 7 Yokozeki K & Hara S (2005) A novel and efficient enzymatic method for the production of peptides from

- unprotected starting materials. *J Biotechnol* **115**, 211–220.
- 8 Arima J, Morimoto M, Usuki H, Mori N & Hatanaka T (2010) β -Alanyl-peptide synthesis by *Streptomyces* S9 aminopeptidase. *J Biotechnol* **147**, 52–58.
 - 9 Arima J, Morimoto M, Usuki H, Mori N & Hatanaka T (2010) The aminolysis reaction of *Streptomyces* S9 aminopeptidase promotes the synthesis of diverse prolyl dipeptides. *Appl Environ Microbiol* **76**, 4109–4112.
 - 10 Arima J, Chiba M, Ichiyangi T, Yabuta Y, Mori N & Aimi T (2010) Eryngase: a *Pleurotus eryngii* aminopeptidase exhibiting peptide bond formation activity. *Appl Microbiol Biotechnol* **87**, 1791–1801.
 - 11 Arima J, Tanaka A, Morimoto M & Mori N (2013) Mutation of active site serine residue with cysteine displays change in acyl-acceptor preference of β -peptidyl aminopeptidase from *Pseudomonas aeruginosa* PAO1. *Appl Microbiol Biotechnol* **98**, 1631–1640.
 - 12 Frère JM (2004) *Streptomyces* R61 D-Ala-D-Ala carboxypeptidase. In *Handbook of Proteolytic Enzymes*, 2 edn (Barrett AJ, Rawlings ND & Woessner JF, eds), pp. 1959–1962. Elsevier, London.
 - 13 Kato Y, Asano Y, Nakazawa A & Kondo K (1989) First stereoselective synthesis of D-amino acid alkyl amide catalyzed by D-aminopeptidase. *Tetrahedron* **45**, 5743–5754.
 - 14 Kato Y, Asano Y, Nakazawa A & Kondo K (1990) Synthesis of D-alanine oligopeptides catalyzed by D-aminopeptidase in non-aqueous media. *Biocatalysis* **3**, 207–215.
 - 15 Kelly JA & Kuzin AP (1995) The refined crystallographic structure of a DD-peptidase penicillin-target enzyme at 1.6 Å resolution. *J Mol Biol* **254**, 223–236.
 - 16 Bompard-Gilles C, Remaut H, Villeret V, Prangé T, Fanuel L, Delmarcelle M, Joris B, Frère J & Van Beeumen J (2000) Crystal structure of a D-aminopeptidase from *Ochrobactrum anthropi*, a new member of the ‘penicillin-recognizing enzyme’ family. *Structure* **8**, 971–980.
 - 17 Okazaki S, Suzuki A, Komeda H, Yamaguchi S, Asano Y & Yamane T (2007) Crystal structure and functional characterization of a D-stereospecific amino acid amidase from *Ochrobactrum anthropi* SV3, a new member of the penicillin-recognizing proteins. *J Mol Biol* **368**, 79–91.
 - 18 Lobkovsky E, Billings EM, Moews PC, Rahil J, Pratt RF & Knox JR (1994) Crystallographic structure of a phosphonate derivative of the *Enterobacter cloacae* P99 cephalosporinase: mechanistic interpretation of a β -lactamase transition-state analog. *Biochemistry* **33**, 6762–6772.
 - 19 Delmarcelle M, Boursoit MC, Filée P, Baurin SL, Frère JM & Joris B (2005) Specificity inversion of *Ochrobactrum anthropi* D-aminopeptidase to a D, D-carboxypeptidase with new penicillin binding activity by directed mutagenesis. *Protein Sci* **14**, 2296–2303.
 - 20 Arima J, Ito H, Hatanaka T & Mori N (2011) Aminolytic reaction catalyzed by D-stereospecific amidohydrolases from *Streptomyces* spp. *Biochimie* **93**, 1460–1469.
 - 21 Arima J, Hatanaka T & Mori N (2011) One-pot synthesis of diverse DL-configuration dipeptides by a *Streptomyces* D-stereospecific amidohydrolase. *Appl Environ Microbiol* **77**, 8209–8218.
 - 22 Dubus A, Ledent P, Lamotte-Brasseur J & Frère JM (1996) The roles of residues Tyr150, Glu272, and His314 in class C β -lactamases. *Proteins* **25**, 473–485.
 - 23 Lamotte-Brasseur J, Dubus A & Wade RC (2000) pKa calculation for class C β -lactamases: the role of Tyr150. *Proteins* **40**, 23–28.
 - 24 Silvaggi NR, Anderson JW, Brinsmade SR, Pratt RF & Kelly JA (2003) The crystal structure of phosphonate-inhibited D-Ala-D-Ala peptidase reveals an analogue of a tetrahedral transition state. *Biochemistry* **42**, 1199–1208.
 - 25 Lee W, McDonough MA, Kotra L, Li ZH, Silvaggi NR, Takeda Y, Kelly JA & Mobashery S (2001) A 1.2-Å snapshot of the final step of bacterial cell wall biosynthesis. *Proc Natl Acad Sci USA* **98**, 1427–1431.
 - 26 Kuzin AP, Liu H, Kelly AJ & Knox JR (1995) Binding of cephalothin and cefotaxime to D-Ala-D-Ala-peptidase reveals a functional basis of a natural mutation in a low-affinity penicillin-binding protein and in extended-spectrum β -lactamases. *Biochemistry* **34**, 9532–9540.
 - 27 Llinás A, Ahmed N, Cordaro M, Laws AP, Frère JM, Delmarcelle M, Silvaggi NR, Kelly JA & Page MI (2005) Inactivation of bacterial DD-peptidase by beta-sultams. *Biochemistry* **44**, 7738–7746.
 - 28 Asano Y, Mori T, Hanamoto S, Kato Y & Nakazawa A (1989) A new D-stereospecific amino acid amidase from *Ochrobactrum anthropi*. *Biochem Biophys Res Commun* **162**, 470–474.
 - 29 Asano Y, Nakazawa A, Kato Y & Kondo K (1989) Properties of a novel D-stereospecific aminopeptidase from *Ochrobactrum anthropi*. *J Biol Chem* **264**, 14233–14239.
 - 30 Asano Y, Ito H, Dairi T & Kato Y (1996) An alkaline D-stereo-specific endopeptidase with β -lactamase activity from *Bacillus cereus*. *J Biol Chem* **271**, 30256–30262.
 - 31 Arthur M, Depardieu F, Cabanié L, Reynolds P & Courvalin P (1998) Requirement of the VanY and VanX D, D-peptidases for glycopeptide resistance in enterococci. *Mol Microbiol* **30**, 819–830.
 - 32 Goffin C & Ghuysen JM (1998) Multimodular penicillin-binding proteins: an enigmatic family of orthologs and paralogs. *Microbiol Mol Biol Rev* **62**, 1079–1093.

- 33 Reynolds PE, Depardieu F, Dutka-Malen S, Arthur M & Courvalin P (1994) Glycopeptide resistance mediated by enterococcal transposon Tn1546 requires production of VanX for hydrolysis of D-alanyl-D-alanine. *Mol Microbiol* **13**, 1065–1070.
- 34 Silvaggi NR, Josephine HR, Kuzin AP, Nagarajan R, Pratt RF & Kelly JA (2005) Crystal structures of complexes between the R61 DD-peptidase and peptidoglycan-mimetic beta-lactams: a non-covalent complex with a 'perfect penicillin'. *J Mol Biol* **345**, 521–533.
- 35 Laemmli UK (1970) Cleavage of structural proteins during the assembly of the head of bacteriophage T4. *Nature* **227**, 680–685.
- 36 Otwinowski Z & Minor W (1997) Processing of X-ray diffraction data collected in oscillation mode. *Methods in Enzymology*, 276, *Macromolecular Crystallography*, part (Carter ACW Jr & Sweet RM, eds), pp. 307–326. Academic Press, New York.
- 37 Leslie AGW & Powell HR (2007) *Evolving Methods for Macromolecular Crystallography*. Springer, Dordrecht. **245**, pp. 41–51. ISBN 978-1-4020-6314-5.
- 38 McCoy AJ, Grosse-Kunstleve RW, Adams PD, Winn MD, Storoni LC & Read RJ (2007) Phaser crystallographic software. *J Appl Crystallogr* **40**, 658–674.
- 39 Adams PD, Afonine PV, Bunkóczi G, Chen VB, Davis IW, Echols N, Headd JJ, Hung L-W, Kapral GJ, Grosse-Kunstleve RW *et al.* (2010) PHENIX: a comprehensive Python-based system for macromolecular structure solution. *Acta Crystallogr D* **66**, 213–221.
- 40 Pettersen EF, Goddard TD, Huang CC, Couch GS, Greenblatt DM, Meng EC & Ferrin TE (2004) UCSF Chimera – a visualization system for exploratory research and analysis. *J Comput Chem* **25**, 1605–1612.
- 41 Chen VB, Arendall WB 3rd, Headd JJ, Keedy DA, Immormino RM, Kapral GJ, Murray LW, Richardson JS & Richardson DC (2010) MolProbity: all-atom structure validation for macromolecular crystallography. *Acta Crystallogr D Biol Crystallogr* **66**, 12–21.